Computation of Periodic Instability of Stratified Fluid Using Continuous Vortex Sheet Dynamics [1]

Zhimin Hu [2] and Stéphan T. Grilli [3]

Abstract

A new model is proposed to compute the time evolution of the interface between two inviscid fluids moving with uniform velocity, subjected to instabilities of the Kelvin-Helmholtz (KH) type. In this model, the interface is represented by a Continuous Vortex Sheet (CVS) which both preserves the full nonlinearity of interfacial boundary conditions and provides a higher-order representation of the geometry and field variables than in previously proposed models. Time updating of CVS's geometry and circulation is calculated as a function of gravity, interfacial surface tension, and fluid density difference. An intrinsic variable expansion technique is introduced to deal with the hyper-singularity occurring in the Biot-Savart integrals describing CVS's velocity. The model is applied to predict the nonlinear growth of periodic KH instabilities in a two fluid stratified system. Results demonstrate that the CVS representation provides both higher numerical accuracy and stability and gives a more accurate physical picture of the disturbance evolution than less accurate methods, like point vortex models, used in earlier analyses.

keywords : continuous vortex sheet, stratified fluid instability, KH instability

1 Introduction

In stratified inviscid flow problems, predicting the time evolution of two-dimensional (2D) interfaces between fluids is of fundamental importance to understanding the larger scale behavior of the flow. In numerical models, this is usually done using 2D shear layers of small thickness compared to a typical streamwise length scale. So-called *vortex sheets* (VS) are an asymptotic model for thin shear layers and fully represent the circulation along fluid interfaces. The problem is thus reduced to solving the initial-value problem describing the VS motion. Examples of such problems are the much-studied case of roll-up of quasi-2D VS's shed by high aspect ratio wings and the Kelvin-Helmholtz (KH) instability of VS's at the interface between two fluids with velocity jump and/or density difference.

Over the past few decades, many attempts were made to model the velocity of continuous VS's using Biot-Savart (BS) integral equations (e.g., Batchelor, 1967). In such studies, however, one conventional approximation has been to discretize continuous VS's by a finite number of point vortices (e.g., Rosenhead, 1931). Moore (1974) thus developed a point-vortex method and successfully calculated roll-up of VS's. For stratified flows, Zalosh (1976) similarly studied

[1] *To appear in* Proc. 1997 ASME Fluid Engng. Div. Summer Meeting, *Vancouver, Canada, 6/97*
[2] Post-doctoral Fellow, *Ocean Engineering Department, University of Rhode Island, Narragansett, RI 02882, USA*
[3] Associate Prof., same address

interfacial instabilities with a method that included effects of buoyancy and surface tension. Using a similar method, Rangel and Sirignano (1988) predicted the evolution of initially small periodic disturbances at the interface between two fluids of different density and velocity, including surface tension, but not gravity, effects. Despite some success, however, such calculations usually resulted, after a large number of time steps, in non-physical chaotic motion of point vortices. Regridding methods, introduced for instance in the latter study, could reduce but not totally eliminate such instabilities. Problems experienced by point-vortex approximations of VS's can be categorized as follows :

- the numerical evaluation of singular terms in BS integrals is not properly handled by standard numerical integration techniques;
- the VS evolution is improperly modeled at extremity points of the computational domain, defining either periodic boundaries or the intersection between the computational domain and infinite VS's or solid boundaries;
- the geometric representation of VS's and of higher-order interfacial tangential derivatives, based on discretized points, is not sufficiently accurate as time develops;
- results converge poorly or even diverge when the VS discretization is refined and/or when non-uniform point-vortex distributions are used.

All of the above problems are numerical, not physical, in nature and are related to specific aspects of discretization methods and calculation of BS integrals. Moore (1974) in fact showed that both point vortex and piecewise constant vortex approximations[4] rapidly cause roundoff and truncation errors to amplify and lead to the reported chaotic motion which ruins practical calculations.

By a careful analysis of work published to date, Fink and Soh (1978) showed that a point vortex representation implicitly neglects logarithmic terms representing local contributions (i.e., vortex self-induced velocity) to the BS integrals. Moore (1979) further showed that a weak singularity does form, after a critical time, on the discretized VS. Accordingly, the point-vortex approximation only converges up to this critical time. In agreement with Moore, Meiron *et al.* (1982), solving a pure shear flow problem, found a curvature singularity of the VS. Krasny (1986), using discrete Fourier analysis, proved that numerical perturbations due to roundoff errors are responsible for the observed irregular motion of point vortices. Baker and Shelley (1990) examined the behavior of layered VS's, with regard to local sheet circulation induced by density and thickness changes, and showed that, beyond the critical time, the behavior of VS layers becomes irregular.

Due to the problems experienced by classical point-vortex approaches, many researchers have pointed out the need for using higher-order VS representations that would reduce numerical errors and allow to better identify the physical mechanisms governing VS evolution. In this paper, we attempt to do so by developing a higher-order continuous vortex sheet (CVS) model and validating it by calculating periodic KH instabilities of a vertically stratified two-fluid system, with both velocity and density differences. A cubic representation of the geometry and circulation is

[4] Note that both of these approximations have identical physical assumptions except that the latter calculates singular terms in the integrals for local constant VS elements.

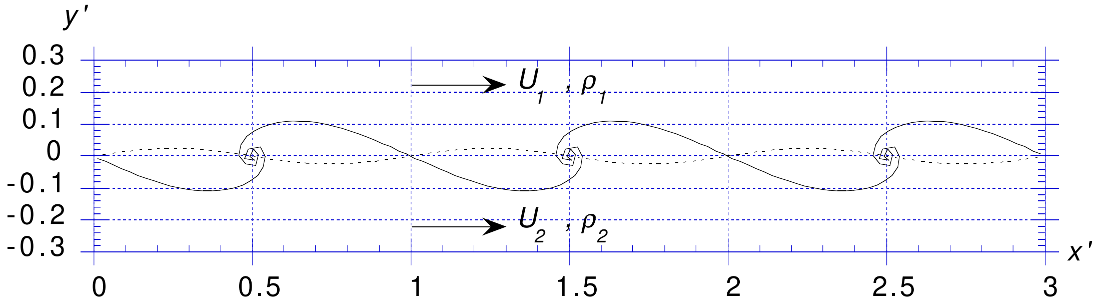

Figure 1: Sketch for periodic Kelvin-Helmholtz (KH) instability with wavelength λ (with, $x' = x/\lambda$, $y' = y/\lambda$). U_1, U_2 are uniform velocities and ρ_1, ρ_2 are densities, for fluids 1 and 2, respectively. Curve (- - - -) is an initial sinusoidal perturbation of amplitude ε on the interface and (——-) is the unstable interface shape computed at a later time.

introduced, based on a piecewise polynomial representation (Boundary Element Method (BEM); Brebbia, 1978), and an explicit time stepping method, based on a 2nd-order Lagrangian Taylor series expansion, is used to calculate CVS's time evolution. At a given time, BS integrals are used to calculate velocities along CVS's. An expansion technique is introduced to deal with the strong singularities occurring in these integrals, as a result of self-induced velocity terms.

2 Periodic KH instability

We consider a vertically stratified system of infinite extension in the x direction, made of two homogeneous inviscid fluids of density ρ_1 and $\rho_2 \geq \rho_1$, moving with uniform horizontal velocity U_1 and U_2, respectively (Fig. 1). An initial sinusoidal disturbance of wavelength λ and small amplitude ε is specified on the interface between both fluids (i.e., $\propto \varepsilon \sin 2\pi x/\lambda$). According to Lamb (1932), the initial vorticity distribution $\gamma(x)$ corresponding to the specified velocity jump, $\Delta U = | U_1 - U_2 |$, is,

$$\gamma(x) = \Delta U \left(1 + 2\pi \frac{\varepsilon}{\lambda} \{ \kappa \sin(2\pi \frac{x}{\lambda}) - 2 \frac{\sqrt{\varphi\,(1-W)}}{(1+\varphi)} \cos(2\pi \frac{x}{\lambda}) \} \right) \tag{1}$$

with,

$$W = \{ (1-\varphi)\frac{g}{k} + \sigma \frac{k}{\rho_1} \} \frac{1+\varphi}{\varphi (\Delta U)^2} \tag{2}$$

where $k = 2\pi/\lambda$ is the wavenumber, g is the acceleration of gravity, $\varphi = \rho_1/\rho_2$, $\kappa = (1-\varphi)/(1+\varphi)$ (the Atwood number), and σ is the interfacial tension coefficient.

This problem was solved by Lamb (1932) in a linear framework (see p. 373 and p. 461). He found that a periodic disturbance would always be unstable and grow exponentially with time as $\propto \exp \omega t$, if $W < 1$ or,

$$\Delta U \; > \; \frac{1+\varphi}{\sqrt{\varphi}}\, c_o \tag{3}$$

with,

$$c_o = \left(\kappa\,\frac{g}{k} + \sigma'\frac{k}{(1+\varphi)}\right)^{1/2} \tag{4}$$

the speed of propagation of interfacial waves, $\sigma' = \sigma/\rho_1$, and,

$$\omega = k\,\Delta U\frac{\sqrt{\varphi\,(1-W)}}{(1+\varphi)} \tag{5}$$

According to Eqs. (2)-(5), the growth of instability will be maximum for a minimum value of c_o. Hence, calculating the critical wavelength leading to this minimum value and replacing it in Eqs. (3) and (4), we obtain the critical velocity jump causing instability (i.e., for which $\omega = 0$ or $W = 1$) as,

$$\Delta U_{cr} = \left(2\frac{1+\varphi}{\varphi}\sqrt{\sigma'\,g\,(1-\varphi)}\right)^{1/2} \tag{6}$$

Lamb's solution assumes that the height of interfacial waves is infinitesimal, which is only an approximation, particularly if the instability is free to develop for a long enough time. As a first approximation, however, Lamb's solution can be used both to predict the threshold velocity likely to cause initial instability of interfacial waves, and the initial stages of growth of instability in the linear regime. Moreover, despite their limitations, Lamb's equations contain the correct physical parameters influencing interfacial instability (i.e., fluid density ratio, interfacial tension, and gravity) that will be used in the numerically exact solution presented hereafter.

In the present model, full nonlinearity of the geometry and flow equations is kept by representing the interface as an inviscid continuous vortex sheet (CVS) whose (complex) motion $z(s,t)$ is given by the Biot-Savart integral equation (Batchelor, 1967),

$$\frac{dz}{dt}(s,t) = u(s,t) - i\,v(s,t) = \frac{i}{2\pi}\int_{-\infty}^{+\infty}\frac{\gamma(s')}{z(s,t)-z(s',t)}\,ds' \tag{7}$$

where, $i = \sqrt{-1}$, $z = x + iy$, and s is the curvilinear coordinate along the VS. The integral in Eq. (7) must be understood in a Cauchy Principal Value (CPV) sense and $\gamma(s)$ is the vortex sheet strength (i.e., circulation), satisfying conservative or non-conservative evolution equations, depending on the problem treated (Rangel and Sirignano, 1988; see next Section).

Due to spatial periodicity of the KH problem, Eq. (7) can be transformed into (Van de Vooren, 1980),

$$\begin{aligned} U(\xi,\eta) &= \frac{d\xi}{d\tau} = \frac{1}{2\lambda}\int_0^{s(\lambda)}\frac{\sinh 2\pi(\eta-\eta')}{\cosh 2\pi(\eta-\eta') - \cos 2\pi(\xi-\xi')}\,\gamma(s')\,ds' \\ V(\xi,\eta) &= \frac{d\eta}{d\tau} = -\frac{1}{2\lambda}\int_0^{s(\lambda)}\frac{\sin 2\pi(\xi-\xi')}{\cosh 2\pi(\eta-\eta') - \cos 2\pi(\xi-\xi')}\,\gamma(s')\,ds' \end{aligned} \tag{8}$$

where dimensionless variables, $\xi = x/\lambda$, $\eta = y/\lambda$, $U = u/\Delta U$, $V = v/\Delta U$, and $\tau = t\,\Delta U/\lambda$, have been used and dashes denote variables calculated at point s' of the VS.

The VS's velocity field (U,V) and motion (ξ,η) induced by a known vorticity distribution can thus be obtained by solving Eq. (8). Due to the nonlinearity in the equations, this can only be performed numerically.

3 Continuous Vortex Sheet model

To calculate the integrals in Eq. (8), following a BEM approach, the CVS geometry over one wavelength is divided into M locally continuous elements, defined using a set of N discretization points. To optimize computations, each of these elements is mapped onto a single reference element, with intrinsic coordinate μ varying between -1 and 1. Hence, summing up element contributions, the velocity induced at time τ, at points $i = 1, ..., N$ of coordinates (ξ_i, η_i) is obtained from Eq. (8) as,

$$\begin{aligned} U_i(\xi_i, \eta_i) &= \frac{1}{2\lambda} \sum_{k=1}^{M} \int_{-1}^{+1} \frac{\gamma(s'(\mu))\, \sinh 2\pi(\eta_i - \eta'(\mu))}{\cosh 2\pi(\eta_i - \eta'(\mu)) - \cos 2\pi(\xi_i - \xi'(\mu))} \frac{ds^k}{d\mu}(\mu)\, d\mu \\ V_i(\xi_i, \eta_i) &= -\frac{1}{2\lambda} \sum_{k=1}^{M} \int_{-1}^{+1} \frac{\gamma(s'(\mu))\, \sin 2\pi(\xi_i - \xi'(\mu))}{\cosh 2\pi(\eta_i - \eta'(\mu)) - \cos 2\pi(\xi_i - \xi'(\mu))} \frac{ds^k}{d\mu}(\mu)\, d\mu \end{aligned} \tag{9}$$

where $ds^k/d\mu$ is the Jacobian of the transformation from element k to the reference element, and the time variable τ has been omitted for simplicity. Integrals in (9) will be calculated by numerical integration (see next Section).

Once known the velocity field at time τ, both the location of material (discretization) points and their updated circulation are found at a later time $\tau + \Delta\tau$ using a truncated Taylor series as,

$$\begin{aligned} \xi_i(\tau + \Delta\tau) &= \xi_i(\tau) + \Delta\tau\, U_i(\tau) + \frac{(\Delta\tau)^2}{2} \frac{dU_i}{d\tau}(\tau) + \mathcal{O}[(\Delta\tau)^3] \\ \eta_i(\tau + \Delta\tau) &= \eta_i(\tau) + \Delta\tau\, V_i(\tau) + \frac{(\Delta\tau)^2}{2} \frac{dV_i}{d\tau}(\tau) + \mathcal{O}[(\Delta\tau)^3] \\ \Gamma_i(\tau + \Delta\tau) &= \Gamma_i(\tau) + \Delta\tau \frac{d\Gamma_i}{d\tau}(t) + \frac{(\Delta\tau)^2}{2} \frac{d^2\Gamma_i}{d\tau^2}(t) + \mathcal{O}[(\Delta\tau)^3] \end{aligned} \tag{10}$$

where $\Gamma_i = \gamma_i/\Delta U$ is the non-dimensional circulation and $(dU_i/d\tau, dV_i/d\tau)$ the accelerations at point i of the CVS. The latter are calculated based on Lagrangian time derivatives of Eqs. (9).

In our study of interfacial instabilities, following Zalosh (1976), Rottman and Olfe (1977), and Rangel and Sirignano (1988), effects of surface tension, gravity, inertia, and density differences will be included when calculating the time evolution of circulation along the interface in Eq. (10). Doing so, we will define a non-conservative system in which circulation can be created or destroyed. Hence, we get,

$$\frac{d\Gamma_i}{d\tau} = 2\kappa \left(\frac{dU_{is}}{d\tau} + \frac{\Gamma_i}{4} \frac{\partial \Gamma_i}{\partial \mathrm{s}} \right) + 2\,\mathbf{Fr}^{-2} \sin\beta_i - 2\,\mathbf{We}^{-1} \frac{\partial \mathrm{c}_i}{\partial \mathrm{s}} \tag{11}$$

in which, $\mathrm{s} = s/\lambda$ and $\mathrm{c}_i = \lambda \partial\beta/\partial s$ are dimensionless variables, **Fr** denotes the Froude number,

$$\mathbf{Fr} = \frac{\Delta U}{\sqrt{g\kappa\lambda}} \tag{12}$$

and **We** denotes the Weber number,

$$\mathbf{We} = \frac{\rho_2 \lambda (1 + \varphi)(\Delta U)^2}{\sigma} \tag{13}$$

The non-dimensional tangential acceleration at the interface is found as,

$$\frac{d\,U_{is}}{d\,\tau} = \frac{d\,U_i}{d\,\tau}\cos\beta_i + \frac{d\,V_i}{d\,\tau}\sin\beta_i \tag{14}$$

Second-order time derivatives of vorticity density, needed in Eq. (10), are obtained by backward finite differences of first-order derivatives calculated with Eqs. (11)-(14). The value of time step $\Delta\tau$ used in the model is adaptively calculated as a function of a constant mesh Courant number ($\simeq$ 0.5), based on maximum tangential velocity and minimum distance between nodes on the interface (Grilli and Subramanya, 1995, 1996).

4 Discretization

4.1 Element selection and parametric representation

Using a BEM, the geometry and field variables (i.e., circulation) of each element are represented by a set of m locally continuous polynomial shape functions $N_j(\mu)$, analytically defined on the reference element using m discretization points (nodes). Hence,

$$x(\mu) = \sum_{j=1}^{m} N_j(\mu) x_j \quad ; \quad y(\mu) = \sum_{j=1}^{m} N_j(\mu) y_j \quad ; \quad \gamma(\mu) = \sum_{j=1}^{m} N_j(\mu)\gamma_j \tag{15}$$

where x_j, y_j, and γ_j are coordinates and circulation for the element nodes, respectively. Derivatives with respect to the intrinsic coordinate (denoted by μ indices) are easily obtained from Eq. (15), using derivatives of shape functions.

Key flow parameters of VS's evolution are functions of tangential s-derivatives of the interfacial slope angle β and curvature $\partial\beta/\partial s$ (e.g., surface tension in Eq. (11)). For each boundary element, these can be expressed as,

$$\cos\beta = \frac{x_\mu}{s_\mu} \quad ; \quad \sin\beta = \frac{y_\mu}{s_\mu} \quad ; \quad s_\mu = \{x_\mu^2 + y_\mu^2\}^{1/2} \tag{16}$$

$$\begin{aligned} \frac{\partial\beta}{\partial s} &= \frac{y_{\mu\mu}\,\cos\beta - x_{\mu\mu}\,\sin\beta}{s_\mu^2} \\ \frac{\partial^2\beta}{\partial s^2} &= \frac{y_{\mu\mu\mu}\,\cos\beta - x_{\mu\mu\mu}\,\sin\beta}{s_\mu^3} - \frac{3}{2\,s_\mu^4}\left[\,2\,x_{\mu\mu}y_{\mu\mu}\,\cos 2\beta - (x_{\mu\mu}^2 - y_{\mu\mu}^2)\,\sin 2\beta\,\right] \end{aligned} \tag{17}$$

which can easily be calculated using derivatives of Eq. (15). Hence, $(x(\mu), y(\mu))$, $\gamma(\mu)$, and s_μ^k, calculated with Eqs. (15) and (16), for each element k, can be substituted into the BS integrals (9). Similarly, these and $\partial^2\beta/\partial s^2$ calculated with Eq. (17) can be substituted into Eq. (11).

4.2 Element parity mapping

As mentioned before, in most earlier models based on point vortices, investigators reported that, as time increases, computations become gradually unstable and, eventually, lead to irregular motion of discretization points (e.g., Moore 1974; Zalosh, 1976; Meiron *et al.*, 1982). Such instabilities are particularly strong when surface tension effects are included (Rangel and Sirignano, 1988). In most of the previously reported work, after experiencing such problems, it was concluded that numerical instabilities were likely due to improper calculation/representation of VS motion in the models. In some work, it was thus attempted, but with little success, to reduce numerical instabilities by improving singular integration calculations. A detailed analysis of the problem showed that irregular motions are always associated with an increasingly poor accuracy of the VS geometric representation and, particularly, of tangential s-derivatives. When KH instabilities develop, intense roll-up of VS's indeed occurs (Fig. 1), leading to large curvature of the interface and to enhanced surface tension effects. Hence, even if a lower-order shape function representation may be acceptable for the circulation, a higher-order representation of the geometry is needed to ensure continuity of inter-element slope and curvature. This was also concluded by Grilli and Svendsen (1990), who used cubic splines, and by Grilli and Subramanya (1995, 1996), who introduced a fourth-order sliding polynomial interpolation of the geometry, independent of the BEM shape functions, to calculate s-derivatives in their computations of overturning surface waves.

In the present study, following Grilli and Subramanya (1995, 1996), a five-node sliding interpolation of the geometry was first tested (i.e., 4th-order isoparametric boundary element in which geometric characteristics are calculated for the middle node of the element). Slope angle and tangential derivatives were calculated by direct differentiation in the sliding element, using Eqs. (15)-(17) with $m = 5$. To calculate characteristics for the next node along the VS, the sliding element was moved forward by one node. The element was kept identical for the first 3 nodes and for the last 3 nodes on the sheet. When using this sliding element for the KH problem, however, after providing the initial trend of VS roll-up, computations rapidly failed and led to irregular motion of nodes, independent of flow conditions and physical properties. A repetition of these calculations using cubic splines did not improve results.

To better identify the nature of instabilities, both the sliding and spline element methods were used to calculate tangential derivatives for a simple sinusoidal interface. We found that :

- the accuracy of tangential derivatives is function of the location of nodes on the interface, especially if the order of derivatives is high;
- the numerical instability or irregular motion of nodes is first triggered by inaccuracies in the higher-order s-derivatives, mostly at locations where a fairly non-uniform distribution of nodes occurs within one element.

These findings also explain why, for the periodic KH problem, instabilities are first observed at the extremity nodes and in roll-up regions of the interface, where the periodic boundary condition is enforced and interface node spacing is most changed, respectively.

A careful analysis of these and similar results showed that the mapping of geometric elements, with irregular node spacing, to a reference element, with constant node spacing, is at the origin

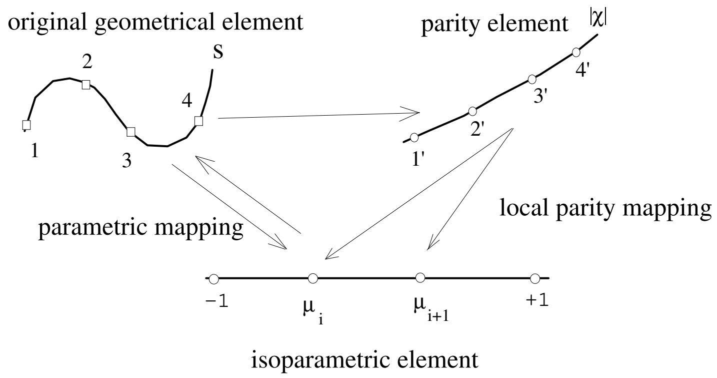

Figure 2: The Parity Mapping scheme for local isoparametric element

of small disturbances in higher-order derivatives which, through time updating, rapidly propagate and lead to sawtooth instabilities of the interface geometry. A new method, referred to as *parity mapping*, was thus designed to provide s-derivatives less dependent on discretization node density. Bases for this method are indicated in Fig. 2. In standard isoparametric element transformation, the distance between nodes in the reference element is constant. In Fig. 2, for instance, with a four-node element, it is equal to two-third. In the parity mapping method, a new (monotonous) mapping variable χ is defined, in between the transformation from s to μ, to create an element with node density similar to the geometric element. The parity element is then mapped onto a reference element with intrinsic coordinate μ varying between [-1,+1] and irregular node spacing. Results show that this method eliminates (or at least greatly reduces) fluctuations induced in tangential derivatives by irregular node spacing.

The parity coordinate χ is defined such as to carry the basic geometric information from the original node distribution, as,

$$\chi_j = \chi_{j-1} + \sqrt{\mid x_j \mid + \mid y_j \mid} \quad ; \; j = 1, ..., m-1 \tag{18}$$

for a m-node isoparametric element ($m \geq 4$ and even). With the middle interval in the element starting at node $i = m/2$, the mapping interval in the reference element is, $\Delta\mu = \mu_m - \mu_1 = 2$, and the corresponding interval in the parity mapping element is,

$$\Delta\chi = \chi_m - \chi_1 = \sum_{j=1}^{m-1} \Delta\chi_j \quad \text{with} \quad \Delta\chi_j = \chi_{j+1} - \chi_j \tag{19}$$

The basic relationship for the parity mapping transformation expresses a geometric scale similarity between χ and μ, as,

$$\Delta\mu_j = \Delta\chi_j \frac{\Delta\mu}{\Delta\chi} \quad ; \; j = 1, ..., m-1 \tag{20}$$

For the 4-node element in Fig. 2, using Eq. (20), we thus have,

$$\mu_i \quad = \quad \Delta\chi_i \frac{2}{\Delta\chi} - 1$$

$$\mu_{i+1} \quad = \quad \frac{2}{\Delta\chi}(\Delta\chi_i + \Delta\chi_{i+1}) - 1 \tag{21}$$

with $\Delta\chi$, $\Delta\chi_i$, and $\Delta\chi_{i+1}$ being given by Eqs. (18),(19).

In the applications, the parity mapping method is used to calculate s-derivatives, based on 5-node 4th-order elements. Other variables needed for the BS integrals are discretized using 4-node cubic sliding boundary elements, in which the middle interval only is used to interpolate in between two nodes (*mid-interval interpolation*; Grilli and Subramanya, 1996).

4.3 Node regridding

When VS's roll-up, some regions of the interface are significantly stretched, which leads to lower node density that may affect accuracy. In other regions, nodes tend to concentrate which may lead to quasi-singular situations, particularly when point-vortices are used. In earlier work, to prevent point vortices from excessively concentrating in roll-up regions of the interface, node regridding methods were used (e.g., by Rangel and Sirignano, 1988) : following the increased length of the interface with time, nodes were adaptively added and regridded to equal arc-length spacing, in order to satisfy a minimum spatial resolution requirement.

In the present model, a similar node regridding technique is used, based on the method developed by Grilli and Subramanya (1996) to study breaking surface waves, which combines cubic spline elements and the new parity mapping interpolation method.

5 Singular integrations

The kernel of BS integrals (9) for each element becomes strongly singular when the observation node i coincides with one node of the integrated element k. The CPV of this integral must thus be properly evaluated. For a two-dimensional problem, as indicated by Eq. (7), the singularity is $\mathcal{O}(1/r)$, where r denotes the distance to point i.

The strong singularity in the integrand, say $F(\mu) = N_j(\mu)s^k_\mu(\mu)f_i(\mu)$, for each element discretized with Eq. (15), can be "extracted" by means of a Laurent series expansion around the singular point (x_i, y_i), of the form (Guiggiani *et* al., 1992),

$$F(\rho,\theta) = \frac{F_{-1}(\theta)}{\rho} + \mathcal{O}(1) \tag{22}$$

where (ρ, θ) denote polar coordinates centered on point i in the reference element and $F_{-1}(\theta)$ is only function of the VS geometry around point i. Thus, the integrals in Eq. (9) for element k (transformed into the intrinsic element) take the form,

$$\begin{aligned} I^k &= \int_{-1}^{+1} F(\rho(\mu),\theta(\mu))\, d\mu \\ &= \int_{-1}^{+1} \{\, F(\rho(\mu),\theta(\mu)) - \frac{F_{-1}(\theta(\mu))}{\rho(\mu)} \,\}\, d\mu + \int_{-1}^{+1} \frac{F_{-1}(\theta(\mu))}{\rho(\mu)}\, d\mu \end{aligned} \tag{23}$$

According to expansion (22), the first integral in Eq. (23) is regular and can thus be calculated by standard Gauss quadrature. The second integral, I_s^k, is divided into three parts, by defining a semi-circular boundary of vanishing radius ϵ centered on the singular point of intrinsic coordinate μ_i, as,

$$\begin{aligned} I_s^k &= \lim_{\epsilon \to 0} \Big\{ -\int_{\mu_i+1}^{\epsilon} \frac{F_{-1}(\pi)}{\rho}\, d\rho - \int_{\pi}^{0} \frac{F_{-1}(\theta)}{\epsilon} \epsilon \sin\theta \, d\theta + \int_{\epsilon}^{-\mu_i+1} \frac{F_{-1}(0)}{\rho}\, d\rho \Big\} \\ &= F_{-1}(0) \ln \frac{1-\mu_i}{1+\mu_i} + \int_0^{\pi} F_{-1}(\theta) \sin\theta \, d\theta \end{aligned} \tag{24}$$

where, by definition, on the intrinsic element, $\mu = \mu_i + \rho \cos\theta$. In (24) the property, $F_{-1}(\theta) = -F_{-1}(\theta + \pi)$ has been used to combine the first and last integrals (Guiggiani *et al.*, 1992).

The calculation of $F_{-1}(\theta)$ first requires defining a local intrinsic coordinate expansion for, $\mathbf{x} - \mathbf{x}_i$, where $\mathbf{x}_i$ denotes the singular point and $\mathbf{x}$ a boundary point, both on element k. Using the same polar coordinates as above, we get,

$$\mathbf{x}(\mu) - \mathbf{x}_i(\mu) = \rho(\mu)\mathbf{A}(\theta(\mu)) + \mathcal{O}(\rho^2) \tag{25}$$

with,

$$\mathbf{A}(\theta) = \frac{\partial \mathbf{x}}{\partial \mu} |_{\mu=\mu_i} \; \{\cos\theta - \tan\theta \sin\theta + \frac{\tan^2\theta}{2} [\frac{d\rho}{d\mu} - \frac{1}{\cos\theta}] \} \tag{26}$$

Using Eqs. (25),(26), we then express various parts of the kernel $F(\mu)$ of BS Eqs. (9) and put it in the form of expansion (22). Finally, all terms are expressed as a function of element shape functions and nodal values, using Eqs. (15)-(17). Details are left out due to lack of space.

6 Applications

The periodic KH instability of a two fluid vertically stratified system will be solved with the model (Fig. 1). A sinusoidal perturbation with small amplitude ε is prescribed on the interface; the initial circulation $\gamma(x)$ is given by Eq. (1). The CVS is discretized with N equally spaced nodes per wavelength λ.

A (very unstable) pure shear flow problem is first considered, with a velocity jump $\Delta U = 0.5$ m/s applied between two layers of an identical inviscid fluid of uniform density ρ (whose absolute value has no influence in the present case). The amplitude of perturbation is $\varepsilon = 0.0025$ m. In Eqs. (1),(2), we have $\varphi = 1$ and $W = \kappa = \sigma = 0$. Eq. (5) also shows that the linear growth of instability is $\omega = k\Delta U/2$ and, in Eq. (11), we can see that $d\gamma/dt = 0$. Hence, as expected for this case, the CVS system is conservative. Model results are given in Fig. 3. The initial discretization has $N = 45$ equally space nodes per wavelength and nodes are added and regridded at each time step, in order to maintain a constant spatial resolution as the CVS length increases when the instability develops.

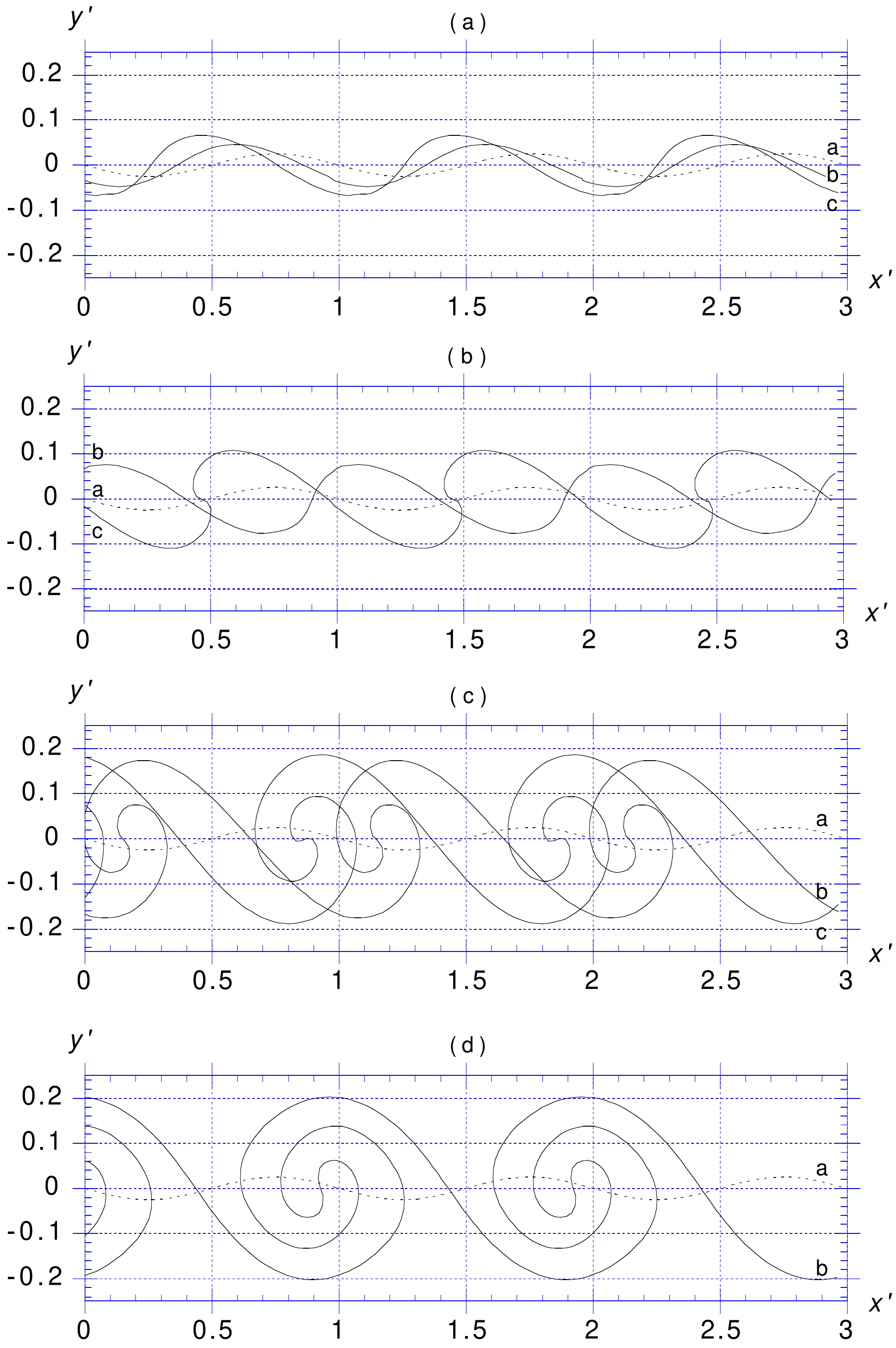
(a)
(b)
(c)
(d)
y'
x'
0.2
0.1
0
-0.1
-0.2
0
0.5
1
1.5
2
2.5
3
a
b
c

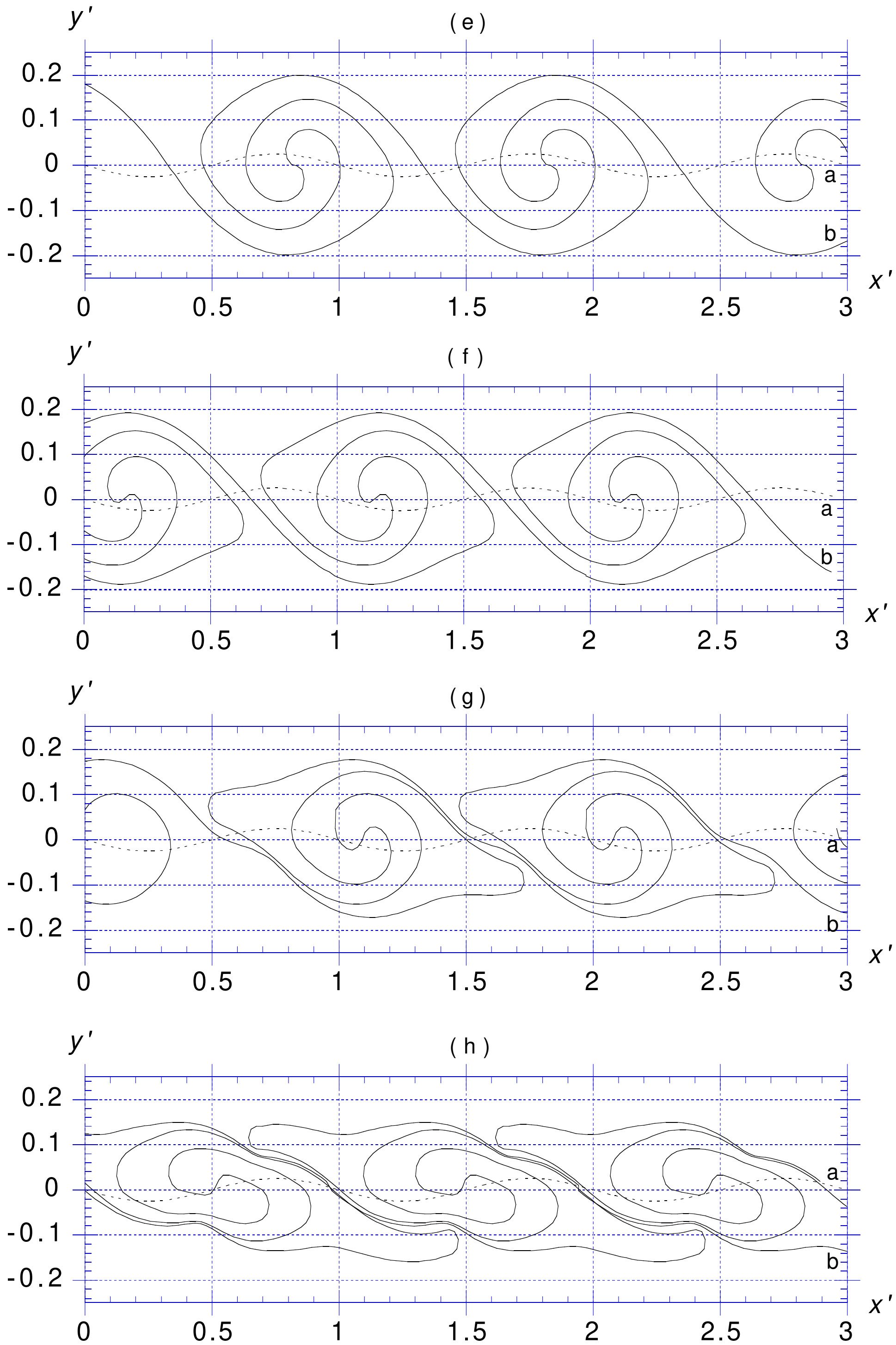

Figure 3: Results for periodic KH instability with wavelength $\lambda = 0.1$m, $|\ \Delta U\ | = 0.5$m/s, $\varphi = 1$, and $\sigma = 0$. curves show interfacial shape at time τ = (a) a : 0.001, b : 0.301, c : 0.601; (b) a : 0.001, b : 0.751, c : 1.201; (c) a : 0.001, b : 1.651, c : 1.951; (d) a : 0.001, b : 2.401; (e) a : 0.001, b : 2.551; (f) a : 0.001, b : 2.701; (g) a : 0.001, b : 2.851; (h) a : 0.001, b : 3.001.

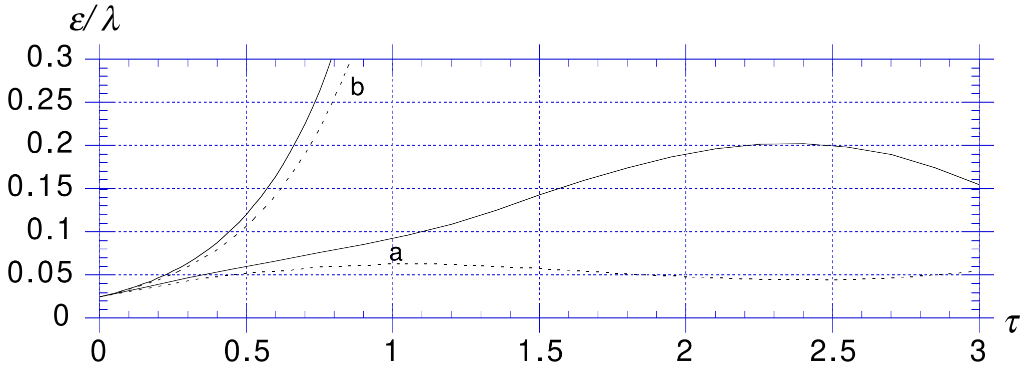

Figure 4: Periodic KH instability with wavelength $\lambda = 0.1$m and $\mid \Delta U \mid = 0.5$m/s : (——) $\varphi = 1$, $\sigma = 0$; (- - - - -) $\varphi = 0.9$, $\sigma = 0.0237$N/m. Curves show the maximum dimensionless amplitude of the interface ε/λ as a function of τ for : (a) CVS model; and (b) linear theory (Lamb, 1932).

Hence, after 3,000 time steps, at the end of computations, the number of nodes increases up to $N = 328$ (last curve in Fig. 3h). The wavelength is selected to $\lambda = 0.1$ m, corresponding to an instability at the ripple scale; the wavelength however does not matter in this problem and results would be self-similar for another wavelength. In order to ensure high accuracy in these very unstable computations, the initial time step is selected to a very small value, $\Delta\tau_o = 0.001$, which corresponds to an initial mesh Courant number of 0.023. Since the spatial resolution is maintained constant through regridding, the time step also stays constant.

Overall, results show reasonable predictions of VS evolution. Fig. 3a shows that, for small time, the interface perturbation slowly grows up while more or less preserving its initial shape; hence, this is referred to as a *quasi-linear* regime. At the same time, a relative motion of crests is observed; this phenomenon, which is not observed in point-vortex models (e.g., Rangel and Serignano (1988); Grilli *et al.*, 1996), indicates that, as the instability develops, interfacial waves travel at a modified phase velocity. In Fig. 3b it is seen that, after the quasi-linear initial growth, the larger nonlinearity in the flow field leads to both increased wave amplitude and skewness and, eventually, to a crest overturning similar to surface wave breaking; this is referred to as the *nonlinear* regime. Comparing Figs. 3a and 3b, it is apparent that for a same time interval of 0.6, the amplitude growth is much larger in the nonlinear regime than in the quasi-linear one. In Fig. 3c, the similarity of results with surface waves disappears as the interface VS starts *rolling -up*. In Figs. 3d-f, as time further increases, the interface roll-up becomes more pronounced. It is worth pointing out that standard point-vortex computations usually fail around the stage of Fig. 3d, whereas the present CVS model provides very stable results for the full stages of development of VS roll-up.

After reaching a maximum value in Fig. 3f, Figs. 3g and 3h show that the amplitude of disturbance starts gradually decreasing, as the "roll-up cells" become more elongated. At this stage, however, it should be pointed out that different fluid regions in the roll-up cells are quite close to each other. Although not creating actual singularities in the flow, such situations lead to highly varying kernels in the BS integrals, that standard Gauss quadrature rules fail to properly integrate unless a prohibitive number of integration points is used. Such integrals, referred to as

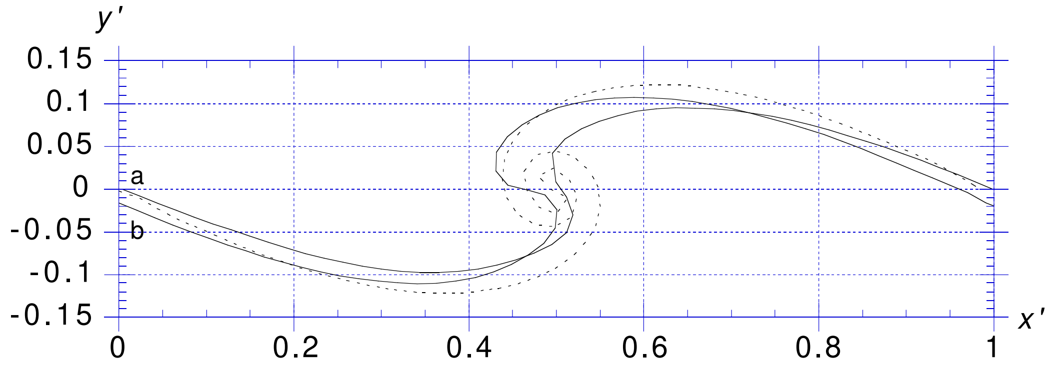

Figure 5: Same case as Fig. 3 : (——) CVS results for (a) $\tau = 1.051$, (b) $\tau = 1.201$; (- - - - -) PCVS results for $\tau = 1.051$.

quasi-singular, thus require more accurate integration methods, usually, as the distance between an observation node i and an element k becomes smaller than, say, 10% of the element length (Grilli and Subramanya, 1994). Quasi-singular integration methods have not yet been implemented in our model. Hence, although no particular instability is observed, one might start questioning result accuracy at and beyond the stage of Fig. 3h.

A second application was carried out for a case with two fluids of different density, $\rho_1 = 0.9$ and $\rho_2 = 1.0$, with surface tension coefficient equal to $\sigma = 0.0237$ N/m (the value for water and oil). The gravitational acceleration was $g = 9.81$ m/s^2. Other parameters, both physical and numerical, were kept to the same value as before. Fig. 4 shows disturbance amplitude growths as a function of time, for both applications, compared to predictions of linear theory from Eq. (5). As could be expected, an increase in interfacial surface tension and a decrease in the upper layer density both reduce the growth rate of nonlinear instability. This was also concluded by Grilli *et al.* (1996) who used a piecewise-constant VS method (PCVS). For both cases, as also observed in earlier studies, linear theory greatly overpredicts the growth rate of instability.

The comparison of PCVS and present CVS results for the first case is given in Fig. 5 for $\tau = 1.051$. Beyond this time, PCVS results become unstable. It is seen that the PCVS model predicts a faster growth of instability than the CVS model. Reasons for the observed differences reside in both a more accurate computation of BS integrals and a better geometric representation in the CVS model. A more detailed understanding of these results, however, still needs to be achieved.

7 Conclusions

A continuous CVS model was proposed for calculating the nonlinear motion of the interface between two inviscid stratified fluids. A BEM methodology was followed to develop higher-order representations of the discretized geometry and circulation in the CVS, which were used to calculate BS integrals for the velocity field. To optimize computations, local integrations of CVS elements were performed in a single reference element. A new parity mapping transformation was proposed to more accurately calculate tangential derivatives in roll-up regions of the CVS. Hypersingular integrations were performed in the reference element, through a Laurent series expansion. The classical periodic Kelvin-Helmoltz instability problem was calculated to validate the new CVS model. Numerical results indicated that : (i) the CVS approximation provides for an accurate and stable numerical solution of the interface time evolution; (ii) the CVS model eliminates the chaotic motion of interface points observed in classical point vortex or piecewise constant VS models, when computations are pushed beyond a critical time. We believe that such chaotic motions may be caused by both inaccuracies in the calculation of BS integrals and improper modeling of VS roll-up when using point vortices; (iii) the time evolution of CVS's significantly differs from the one calculated with point vortices. Beside a different growth rate of instability, disturbance waves on the CVS move with a specific phase velocity, larger than the VS's average velocity. Hence these are traveling rather than standing waves, with respect to the VS. The importance of both of these differences depends on fluid physical properties, velocity, and density difference; (iv) computations of the later stages of CVS evolution indicate that the KH disturbance growth levels up and then decreases. This is likely due to larger deformations in the roll-up regions of the VS, which start tightly spiraling and tilting to the downstream direction, implying that, after this stage, nonlinearity begins to play a more dominant role and prevents further disturbance growth. Instead, energy exchange and redistribution will occur by splitting or reuniting of roll-up sections, inside the VS itself.

Acknowledgment

The authors wish to acknowledge support for this research from the U.S. Department of Transportation (United States Coast Guards District No. 1), Grant No. DTRS-5795-G-00065, FY 1995 Oil Pollution Research Grant Program. The information reported in this work does not necessarily reflect the position of the US Government.

References

1. Baker, G.R. and M.J., Shelley (1990) On the Connection between Thin Vortex Layers and Vortex Sheets. *J. Fluid Mech.*, **215**, 161-194.

2. Batchelor, G.K. (1967) *An introduction to fluid dynamics*. Cambridge University Press.

3. Brebbia, C.A. (1978) *The Boundary Elements Method for Engineers*. John Wiley and Sons.

4. Fink, P.T. and W.K., Soh (1978) A New Approach to Roll-up Calculations of Vortex Sheets. *Proc. Roy. Soc. London*, **A362**, 195.

5. Grilli, S.T., Hu, Z. and Spaulding, M.L. (1996) Numerical Modeling of Oil Containment by a Boom. In *Proc. 19th Arctic and Marine Oil spill Prog. Tech. Seminar* (AMOP), pps. 343-376. Environment Canada.

6. Grilli, S.T. and Subramanya, R. (1994) Quasi-singular Integrations in the Modelling of Nonlinear Water Waves. *Engng. Analys. with Boundary Elements,* **13**(2), 181-191.
7. Grilli, S.T. and Subramanya, R. (1995) Recent Advances in the BEM Modelling of Nonlinear Water Waves. Chapter 4 in *Boundary Element Applications in Fluid Mechanics*, pps. 91-122. Advances in Fluid Mechanics Series. Comp. Mech. Pub., Southampton, UK.
8. Grilli, S.T. and Subramanya, R. (1996) Numerical Modeling of Wave Breaking Induced by Fixed or Moving Boundaries. *Computational Mech.*, **17**(6), 374-391.
9. Grilli, S.T. and I.A., Svendsen (1990) Corner Problems and Global Accuracy in the Boundary Element Solution of Nonlinear Wave Flows. *Engng. Analys. with Boundary Elements*, **7**(4), 178-195.
10. Guiggiani, M., Krishnasamy, G., Rudolphi, T.J., and F.J. Rizzo (1992) A General Algorithm for the Numerical Solution of Hypersingular Boundary Integral Equations. *Trans. ASME*, **59**, 604-614.
11. Krasny, R. (1986) A Study of Singularity Formation in a Vortex Sheet by the Point-vortex Approximation. *J. Fluid Mech.*, **167**, 65-93.
12. Lamb, H. (1932) *Hydrodynamics*. Cambridge University Press, 6th edition.
13. Moore, D.W. (1974) A Numerical Study of the Roll-up of a Finite Vortex Sheet. *J. Fluid Mech.*, **63**(2), 225-235.
14. Moore, D.W. (1979) The Spontaneous Appearance of a Singularity in the Shape of an Evolving Vortex Sheet. *Proc. Roy. Soc. London*, **A365**, 105.
15. Meiron, D.I., Baker, G.R., and S.A. Orszag (1982) Analytic Structure of Vortex Sheet Dynamics. Part 1. Kelvin-Helmholtz Instability. *J. Fluid Mech.*, **114**, 283-298.
16. Rangel, R.H. and W.A., Sirignano (1988) Nonlinear Growth of Kelvin-Helmholtz Instability : Effect of Surface Tension and Density Ratio. *Phys. Fluids*, **31**(7), 1845-1855.
17. Rosenhead, L. (1931) The Formation of Vortices from a Surface of Discontinuity, *Proc. Roy. Soc. London*, **A134**, 170-192.
18. Rottman, J. W. and D.B., Olfe (1977) Comment on "Discretized Simulation of Vortex Sheet Evolution with Buoyancy and Surface Tension Effects". *AIAA J.*, **15**, 1214-1215.
19. Van de Vooren, A.I. (1980) A Numerical Investigation of the Rolling up of Vortex Sheets. *Proc. R. Soc. London*, **A373**, 67-91.
20. Zalosh, R.G. (1976) Discretized Simulation of Vortex Sheet Evolution with Buoyancy and Surface Tension Effects. *AIAA J.*, **14**, 1517-1523.